Atmos. Chem. Phys. Discuss., 9, 19387–19433, 2009
www.atmos-chem-phys-discuss.net/9/19387/2009/

Atmospheric Chemistry and Physics Discussions

This discussion paper is/has been under review for the journal *Atmospheric Chemistry and Physics (ACP)*. Please refer to the corresponding final paper in *ACP* if available.

Modeling of Saharan dust outbreaks over the Mediterranean by RegCM3: case studies

M. Santese[1], M. R. Perrone[2], A. S. Zakey[3], F. De Tomasi[2], and F. Giorgi[3]

[1]CMCC-Centro Euromediterraneo per i Cambiamenti Climatici, 73100 Lecce, Italy
[2]CNISM, Physics Department, Universita' del Salento, 73100 Lecce, Italy
[3]Abdus Salam International Centre for Theoretical Physics, 34100 Trieste, Italy

Received: 10 July 2009 – Accepted: 31 August 2009 – Published: 17 September 2009

Correspondence to: M. Santese (monica.santese@le.infn.it)

Published by Copernicus Publications on behalf of the European Geosciences Union.

Abstract

The regional climate model RegCM3 coupled with a radiatively active aerosol model with online feedback is used to investigate direct and semi-direct radiative aerosol effects over the Sahara and Europe in a test case of July 2003. The aerosol model includes dust particles in addition to sulfates, hydrophobic and hydrophilic black carbon and organic carbon. The role of the aerosol online feedback on the radiation budget and the direct radiative forcing (short-wave and long-wave) by dust particles are investigated by intercomparing results from three experiments: REF, including all interactive aerosol components, Exp1, not accounting for the aerosol radiative feedback, and Exp2 not accounting for desert dust particles. The comparison of results in the REF experiment with satellite observations, sun/sky radiometer measurements, and lidar profiles at selected Central Mediterranean sites reveals that the spatio-temporal evolution of the aerosol optical depth is reasonably well reproduced by the model during the entire month of July. Results for the dust outbreaks of 17 and 24 July, averaged over the simulation domain, show that the daily-mean SW direct radiative forcing by all particles is $-24\,W/m^2$ and $-3.4\,W/m^2$ on 17 July and $-25\,W/m^2$ and $-3.5\,W/m^2$ on 24 July at the surface and top of the atmosphere, respectively. This is partially offset by a LW direct radiative forcing of ~30% at the surface and of ~50% at the ToA. It is also shown that atmospheric dynamics and hence dust production and advection processes are dependent on the simulation assumptions and may significantly change within few tens of kilometers. The comparison of REF and Exp1 shows that the aerosol online feedback on the radiation budget decreases the domain-average daily-mean value of the 2 m-temperature, aerosol column burden (CB), and short-wave (SW) atmospheric forcing by 0.52°C, 14%, and 0.9%, respectively on 17 July and by 0.39°C, 12% and 12%, respectively on 24 July. The comparison of REF and Exp2 reveals that on 17 July, radiatively-active dust particles decrease the daily-mean 2-m temperature averaged over the whole simulation domain by 0.12°C even if are responsible for 99.8% and 97% of the daily-mean aerosol column burden and SW atmospheric forcing,

ACPD

9, 19387–19433, 2009

respectively.

1 Introduction

The influence of aerosols on the Earth's climate is not yet adequately taken into account in climate models. As a consequence, research activities aimed at improving the aerosol representation in climate models are essential for a more accurate prediction of climatic changes. Indeed, an advanced, multi-disciplinary approach that integrates surface and space-based measurements with models needs to be developed to achieve the goal of reducing uncertainties in aerosol impacts on climate (US Climate Change Science Program; Chin et al., 2009). The Mediterranean basin has a particular relevance in aerosol-climate studies, as this area is particularly affected by air pollution. In addition to sea-spray aerosols, mineral dust and biomass burning particles from Northern and Central Africa, long-range transported urban/industrial and biomass burning aerosols from Northern and Eastern Europe converge over the Mediterranean. As a consequence, several studies indicate that the aerosol radiative forcing is among the highest in the world during Mediterranean summers (e.g. Lelieveld et al., 2002; Andreae et al., 2002). In addition, Giorgi (2006) identified the Mediterranean as one of the most responsive regions to GHG-induced global climate change, so that the aerosol forcing is expected to strongly interact with the GHG forcing over this region.

Mineral dust is among the major aerosol components over the Mediterranean, however its radiadive impact is still not well defined. The net perturbation of the radiation balance (solar and terrestrial) imposed by mineral dust (i.e. the dust radiative forcing) is complex (Sokolik et al., 2001) due to its scattering, absorption, and emission properties. Sign and magnitude of the direct dust radiative forcing are controlled by the dust optical properties, which depend on the dust size distribution and refractive index. The latter in turn depends on the mineral composition and particle mixing state, which might vary regionally due to potentially different soil properties of dust source regions (Tegen, 2003). Therefore the net dust radiative forcing (sum of solar and long-wave)

ACPD
9, 19387–19433, 2009

exhibits large regional variations, which makes it difficult to estimate a global mean.

The recent development of high-resolution regional climate models (RCMs) offers a useful tool to assess the regional impacts of aerosols, including mineral dust (e.g. Zakey et al., 2006; Perez et al., 2006; Heinold et al., 2007). Compared to General Circulation Models (GCMs), the relatively high-resolution and detailed physical parameterizations of RCMs are particularly suitable to describe the complexity of aerosol processes (Solmon et al., 2006). Furthermore, the results from regional models are well suited for comparison with measurements of individual events at selected sites.

In an effort to improve the understanding of mineral dust impacts on regional climate, Zakey et al. (2006) recently developed a radiatively active desert dust module and coupled it to the regional climate model RegCM3 (Version 3.1, Pal et al., 2007), developed at the Abdus Salam International Centre for Theoretical Physics (ICTP) of Trieste (Italy). The dust module, which includes emission, transport, gravitational settling, wet and dry removal and calculations of dust optical properties, has further been improved by Solmon et al. (2008) and Zhang et al. (2009) by including the long-wave radiative forcing. Heinold et al. (2007) also developed a new regional model system (LM-MUSCAT) to estimate the dust direct and semi-direct forcing by means of an online feedback of dust on the model radiation scheme. In addition, Perez et al. (2006) demonstrated the impact of dust-radiation interaction on weather forecast improvements by using the Dust REgional Atmospheric Modeling (DREAM) system.

In this paper, RegCM3 is coupled with a radiatively active aerosol model with online feedback on the radiation scheme following previous studies (Zakey et al., 2006; Konare et al., 2008; Todd et al., 2008; Zhang et al., 2009), and it is used to investigate the aerosol radiative forcing over the Sahara and central Mediterranean during African dust intrusions. In particular, RegCM3 is used to simulate the test period of July 2003, which includes two significant episodes of mineral dust intrusions from the Sahara onto the central Mediterranean on 17 and 24 July, 2003 (Tafuro et al., 2006). The RegCM3 aerosol module includes, in addition to dust particles, sulphates, hydrophobic and hydrophilic black carbon and organic carbon (Solmon et al. 2006; Zakey et al., 2006).

ACPD
9, 19387–19433, 2009

As mentioned, the Mediterranean basin is characterized by a complex atmospheric chemistry influenced by regional and long-range transported emissions from both continental Europe and the Africa deserts (Santese et al., 2008). Therefore, it is very important to use a model where the contribution of different aerosol components is considered even during dust events. Recent studies at a south-east Italian site (Bellantone et al., 2008) clearly revealed that carbonaceous and sulphate particles were the main components of fine-mode aerosols during dust outbreaks, representing more than 50% of the total aerosol burden.

The RegCM3/aerosol model performance is tested in this paper with case studies by comparison with a range of observations, including satellite products, sun/sky radiometer measurements, and lidar profiles at selected Central Mediterranean sites. After a brief model description is given in Sect. 2, the comparison of observations and model data in the reference (REF) experiment is presented in Sect. 3 and the aerosol radiative effect is analyzed in Sect. 4. In addition to the REF simulation, two experiments are analyzed to highlight both the effects of the aerosol online feedback on the radiation scheme (Sect. 5) and the direct and semi-direct radiative effects by dust particles both at solar and thermal wavelengths (Sect. 6). Summary and conclusion are given in Sect. 7.

2 RegCM3 modeling system

The Regional Climate Model version 3 (RegCM3) used in the present work is a hydrostatic, sigma vertical coordinate model based on the mesoscale model MM5 (Grell et al., 1994), with improvements in various physics packages (Pal et al., 2007). Typical horizontal grid spacings for climate application range from 20 to 80 km. Atmospheric radiative transfer processes at solar (SW) and thermal (LW) wavelengths are from the NCAR global model CCM3 and are described by Kiehl et al. (1996). Land surface processes, which describe the transfer of energy, mass and momentum between the atmosphere and the biosphere, are represented via the Biosphere-Atmosphere Trans-

ACPD
9, 19387–19433, 2009

fer Scheme (BATS1e; Dickinson et al., 1993). Planetary boundary layer computations follow the non-local parameterization of Holtslag et al. (1990). The mass flux scheme of Grell (1993) is used to describe convective precipitation and the sub-grid explicit moisture scheme of Pal et al. (2000) is used to represent non-convective precipitation.

2.1 Anthropogenic aerosol model

The anthropogenic aerosol model implemented within RegCM3 includes prognostic equations for six tracers: the SO_2/SO_4^{2-} system, hydrophobic and hydrophilic black carbon (BC) and organic carbon (OC). Solmon et al. (2006) presents a detailed description of this scheme along with the emission inventories used by the model. Solmon et al. (2006) evaluated the model performance in terms of surface concentrations and aerosol optical depth over a wide and contrasted domain extending from northern Europe to southern sub-tropical Africa at a 60-km spatial grid spacing without considering the aerosol radiative forcing.

2.2 Dust model

The desert dust module implemented within RegCM3 is described in detail by Zakey et al. (2006). It is based on the works of Marticorena and Bergametti (1995) and Alfaro and Gomes (2001) and includes emission, transport, gravitational settling, wet and dry removal, and calculation of dust optical properties. The coupled RegCM3–dust model was tested by simulating a northeastern Africa dust outbreak and a west Africa-Atlantic dust outbreak, as well as by performing a three month simulation over an extended domain covering the Africa-Europe sector. Comparisons with observations gave encouraging indications concerning the use of the dust model for climate applications.

The coupled RegCM3–dust model was used by Konare et al. (2008) and Solmon et al. (2008) to investigate the effect of the short-wave and long-wave radiative forcing of Saharan dust on the west Africa monsoon. It was shown that the short-wave forcing

ACPD
9, 19387–19433, 2009

was dominant in generating a reduction of monsoon northward penetration and precipitation over the Sahel. More recently, the coupled RegCM3–dust model was further implemented by Zhang et al. (2009) to simulate the net radiative forcing (short-wave and long-wave) and related climate effects of dust aerosols over East Asia. The radiative code in the RegCM3 employs the δ-Eddington approximation for radiative flux calculations, and the wavelength spectrum is divided into 18 discrete intervals from 0.2 to 4.5 µm. Seven of these span the ultraviolet (0.2–0.35 µm), one covers the visible (0.35–0.64 µm) and the remaining bands cover the infrared or special absorption windows. Zhang et al. (2009) provide a detailed description of the aerosol parameters used to perform radiative forcing calculations.

2.3 Experiment design

The model domain used in this study covers major parts of the Sahara desert and southern Europe with 100×115 grid points at a horizontal grid spacing of 50 km, with 18 vertical sigma layers and model top at 100 hPa. Figure 1 shows by a color coded plot the sand source percentages within the model domain. Meteorological initial and time-evolving lateral boundary conditions for the RegCM3 simulations are from the National Centers for Environmental Prediction/National Center for Atmospheric Research (NECP/NCAR) re-analysis (Kalnay et al., 1996). The land cover is specified using the Global Land Cover Characterization (GLCC) version 2 data provided by the US Geology Survey (USGS) Earth Resources Observation System Data Center (Loveland et al., 2000). Soil texture data are based on the USDA texture classification (USDA, 1999).

The model simulations extend from 1 to 31 July 2003 in order to capture the main African dust intrusions that occurred over the Mediterranean basin during July 2003. These have been well documented for example by Tafuro et al. (2006). Three simulations are conducted and analyzed. The radiatively active aerosol model with online feedback on the RegCM3 radiation scheme is used for the reference (REF) simulation. The second simulation (Exp1) includes the radiatively active aerosol model, but the

ACPD
9, 19387–19433, 2009

online feedback on the RegCM3 radiation is not accounted for. Finally, in order to examine the contribution of the mineral dust radiative forcing a simulation not accounting for the mineral aerosol component is performed (Exp 2).

3 Model validation

Model results are validated by comparison with aerosol optical depths (AODs) from satellites and sun/sky radiometer measurements and with extinction coefficient vertical profiles obtained from lidar measurements at selected Central Mediterranean sites. The evaluation of individual dust events is a necessary step in order to assess the realism of emission and transport processes in numerical models.

3.1 Overview of July 2003 African dust intrusion episodes

Particularly intense sand storms occurred over northwestern Africa on 4 July, 17 July, and 23–24 July 2003, as revealed by the true-color images from the Sea Wide Field-of-view Sensor (SeaWiFS, http://www.nrlmry.navy.mil/aerosol/) on board of the NASA SeaStar spacecraft (Fig. 2a–d). One picture per day is shown in Fig. 2a–d for the whole Mediterranean region as a composite of the data collected between 11 and 13 UTC along the spacecraft polar orbit (Tafuro et al., 2006). Figure 2 shows that the dust intrusion from the western Sahara extends all the way to the Italian peninsula and western Greece. Figure 3 presents a comparison between the simulated daily mean wind fields at 10 m (a–d) and the corresponding NCEP-NNRP2 reanalysis dataset used for the model initial and lateral boundary conditions interpolated onto the model grid for 4, 17, 23 and 24 July, respectively. The wind patterns are well captured by RegCM3. Daily mean values of dust emission fluxes ($\mu g\,m^{-2}\,s^{-1}$) are reported in Fig. 3i–n by color coded plots for 4, 17, 23 and 24 July, respectively. We observe that the strong wind currents cause intense dust emissions especially over the Algeria/Tunisia/Libya border on 4 July. Western Sahara is the main dust source on 17 July, even if significant

ACPD
9, 19387–19433, 2009

dust sources also are activated over Mauritania and Algeria. Intense dust emissions are especially activated over the Mauritania/Mali/Algeria border on 23 and 24 July.

3.2 Comparison of simulated and observed aerosol optical depths

Figure 2e–h shows by color coded plots the simulated (daily average) total aerosol optical depth (AOD) at the model band 350–640 nm for 4, 17, 23, and 24 July, respectively. Comparison with Fig. 2a–d reveals that RegCM3 catches the spatial distribution of the dust intrusions over the central Mediterranean. The AOD reaches values of up to 6 over the dust source regions (Fig. 3i–n) and decreases to values of up to 1.5 over the Central Mediterranean and the Italian Peninsula.

Daily AOD-mean-values from the model (dotted black lines) are compared in Fig. 4a–e to corresponding daily AOD (solid black lines) retrieved from cloud-screened and quality-assured AERONET sun/sky photometer measurements. More specifically, AOD daily-mean-values at 550 nm retrieved from sun/sky photometer measurements at Lampedusa (35.52° N, 12.63° E), Oristano (39.91° N, 8.5° E), Etna (37.61° N, 15.02° E), Lecce (40.33° N, 18.10° E), and Rome (41.84° N, 12.65° E) are plotted in Fig. 4a–e. These Italian AERONET sites (Fig. 1) have been significantly affected by dust outbreaks in July 2003, as clearly seen in Fig. 2a–d. It is also worth mentioning that we use AERONET daily-mean values of the Angstrom coefficient (440 nm/870 nm) and the AOD at 440 nm to estimate AODs at 550 nm. The uncertainty on AERONET AODs is ±0.01 and is assumed wavelength-independent (Dubovik et al., 2000).

Figure 4 shows a good performance of the model in catching the AOD evolution with time at most sites. The events on 17, 23, and 24 July are captured at Lampedusa, Oristano, Roma and Etna. The event of 4 July is also captured at Lampedusa and Lecce, although the AOD is overestimated in the former case. The AOD is generally underestimated at Lecce, the location farthest away from the dust source regions, suggesting a somewhat weak long range transport by the model. In fact, we observe from Fig. 4 that the differences between model- and observation-based-AODs increase with the distance of the AERONET site from the north-west Africa coast. This result is further il-

ACPD
9, 19387–19433, 2009

lustrated by Fig. 5a–b which show the scatterplot of RegCM3 AODs versus AERONET AODs retrieved (a) at Lampedusa (full dots) and Oristano (open triangles) and (b) at Lecce (rombs), Etna (crosses), and Rome (boxes). The solid black lines in the figures represent the linear regression line fitting the data points. Regression line slope and linear correlation coefficient (R) are also given for each plot in addition to the root mean square (RMS) difference between RegCM3 AODs and the corresponding daily AERONET AODs. We observe from Fig. 5a that the regression line slope is 0.8±0.1 and that R=0.5 at the stations Lampedusa and Oristano closer to the dust source region. Conversely, the regression line slope in Fig. 5b is significantly lower (0.36±0.05) and the data are less correlated (R=0.35) at the stations farther away. These results indicate that on average RegCM3 underestimates AODs and that this underestimation increases with the distance from the dust sources.

The AOD daily mean values retrieved by measurements of the Moderate Resolution Imaging Spectroradiometer (MODIS), onboard of both the EOS Terra and Aqua polar-orbiting satellites (King et al., 1992) are also shown in Fig. 4 (grey solid line). In particular, MODIS Land_Ocean AODs at 550 nm calculated by averaging all data points of a 50×50 km^2 box centered around the AERONET site are plotted. The consistency of MODIS AODs with AERONET AODs is quite satisfactory, even if the AERONET AODs are retrieved from local measurements. Figure 5c–d shows the scatterplot of RegCM3 AODs versus MODIS AODs retrieved (c) at Lampedusa (full dots) and Oristano (open triangles) and (d) at Etna (crosses), Lecce (rombs), and Rome (boxes). Again, the solid black line represents the linear regression fitting the data points. Figure 5c shows that the regression line slope of the Lampedusa-Oristano scatterplot is 0.80±0.09, while the regression line slope in Fig. 5d is 0.33±0.04. In addition, the data points of Fig. 5d are less correlated than those of Fig. 5c. These results thus generally confirm the findings based on the AERONET observations.

In comparing simulated and observed AODs, it should be stressed that a contribution to the differences between simulated and observed AODs is due to the fact that both the AERONET- and MODIS-AODs are representative of the total aerosol load, while the

ACPD
9, 19387–19433, 2009

RegCM3 model only includes few aerosol components (sulfate, black carbon, organic carbon, and dust). The underestimate of sulfate and carbon particle concentrations representing the main anthropogenic aerosol components of local origin and/or long-range transported from industrialized areas (e.g. Bellantone et al., 2008; Santese et al., 2008) may also be responsible for these results. In this respect, it is worth noting from Fig. 4 that AODs larger than 0.05 were found at all AERONET sites on dust-free days, when the simulated AODs were very small. Finally, the uncertainties on dust optical properties that depend on the particle size and refractive indices (Zhang et al., 2009) may also contribute to the differences between RegCM3- and observation-based-AODs.

3.3 Comparison of simulated and lidar-based aerosol vertical profiles

Aerosol extinction coefficient profiles by lidar measurements at Etna and Lecce are compared to corresponding profiles provided by RegCM3 in Figs. 6 and 7, respectively. An elastic-Raman lidar employing a XeF excimer laser has routinely been used during 2003 at the Physics Department of Salento's University, at the suburbs of Lecce, for monitoring aerosol vertical profiles. In particular, Lecce's lidar allows the retrieval of vertical profiles of the aerosol extinction coefficient α_{ext} at 351 nm (De Tomasi and Perrone, 2003). At Mount Etna, a vehicle-mounted lidar system (VELIS, Gobbi, 2000) that employs a Nd:YAG laser has operated from 15 to 31 July 2003. The VELIS lidar allows the retrieval of extinction coefficient vertical profiles at 532 nm (Tafuro et al., 2006).

Figures 6 and 7 show examples of vertical profiles of extinction coefficients on 17 and 24 July at the two locations as observed by lidar and as simulated at the closest model grid point and time. In Fig. 7 lidar profiles at 550 nm are plotted using Angstrom coefficient values retrieved by sun/sky photometer measurements. Relative uncertainties on lidar extinction profiles vary in the range of 5–30%.

Given all the uncertainties underlying the comparison of grid point modeled data and station profiles, the agreement with observations at the Etna site is satisfactory. Con-

ACPD
9, 19387–19433, 2009

versely, at Lecce significantly larger extinction coefficients are found in the lidar data, primarily below 3 km of altitude. The high variability within few hours of the aerosol vertical distribution during Sahara dust outbreaks (e.g. Tafuro et al., 2007), may partially account for the differences between experimental and simulated extinction profiles. However the underestimation at Lecce is consistent with the AOD data of Figs. 4–5. As mentioned, this may be an indication of weak long range transport of dust with a contribution from the underestimate of anthropogenic aerosol amounts. In fact, morphological and elemental analyses on particulate matter samples collected at Lecce show that the anthropogenic fine mode aerosol, mainly composed of nitrate, sulfate, and carbon particles, can represent more than 50% of the aerosol load even during dust outbreaks (Bellantone et al., 2008).

4 Aerosol radiative effect during dust outbreaks: reference simulation

In this section we analyze the short-wave (SW), long-wave (LW), and net aerosol radiative forcing over the model domain during the simulated dust intrusion events. According to IPCC-2007, the level of scientific understanding of the aerosol forcing is medium-low (http://ipcc-wg1.ucar.edu/wg1/wg1_home.html) and a great effort has been dedicated to improve its estimates through dedicated measurement campaigns and integrated analyses (e.g. Yu et al., 2006). The aerosol forcing depends on several parameters such as surface albedo, aerosol layer altitude, aerosol particle median diameter, and aerosol optical thickness. The sign of the radiative forcing is mainly determined by the value of the aerosol single scattering albedo, which is an uncertain parameter in current aerosol radiation models (Helmert et al., 2007). Dust aerosols are large in size and have absorbing properties in the infrared spectral region. Hence, unlike other aerosol species, they also influence the long-wave radiation. Here we specifically analyze results for the dust events of 17 and 24, when a large amount of dust entered the Mediterranean basin (Fig. 4). 17 July daily-mean-values of the SW, LW, and net aerosol forcing at the top of the atmosphere (ToA) and at the surface (sfc)

ACPD
9, 19387–19433, 2009

are shown in Fig. 8a–c and 8d–f, respectively, while corresponding values for 24 July are shown in Fig. 9a–f.

Figures 8a and 9a show that daily mean values of the direct SW-ToA aerosol forcing are on average positive over dust-sources. In particular, the SW-ToA aerosol forcing reaches values up to 50 W/m^2 at the sites where daily mean values of dust emission fluxes ($\mu g\, m^{-2}\, s^{-1}$) are highest. Conversely, the SW-ToA aerosol forcing is on average negative over the Mediterranean areas affected by the dust intrusion and in particular reaches values up to $-40\, W/m^2$ over the Mediterranean Sea. The SW-ToA aerosol forcing varies within the $-(10–5)\, W/m^2$ and the $-(20–5)\, W/m^2$ range on 17 and 24 July, respectively, over the Italian peninsula, which represents the European region mostly affected by July dust intrusions. This change in sign of the SW-ToA aerosol forcing is related to the dependence of mineral aerosol radiative effects on the brightness of the underlying surface (e.g. Balkanski et al., 2007). Over bare surfaces with a high surface albedo (>0.3), such as the Sahara desert, the mineral aerosol tends to warm the atmospheric column by providing a less reflecting layer. Conversely, over dark surfaces, such as ocean and deciduous forests, where the surface albedo is less than 0.15, the effect of the mineral dust is similar to that of sulphates and lead to cooling of the atmospheric column. Therefore, our results show that the cooling effect by aerosol at the ToA is larger over Europe than over the Sahara. In fact, the daily SW-ToA aerosol forcing averaged over Europe and the Mediterranean Sea is −3.9 and $-4.9\, W/m^2$ on 17 and 24 July, respectively (Table 1). Conversely, the daily SW-ToA aerosol forcing averaged over the Sahara is −3.0 and $-2.6\, W/m^2$ on 17 and 24 July, respectively (Table 1).

Figures 8d and 9d show, as expected, that daily mean values of the SW-sfc aerosol forcing are always negative, reaching values of up to $-240\, W/m^2$ at the sites where daily mean values of AODs and dust emission fluxes are highest (Figs. 2–3). On 17 July the SW-sfc aerosol forcing varies within the range of $-(50–20)\, W/m^2$ and $-(20–10)\, W/m^2$, over the central-west Mediterranean Sea and most of the Italian peninsula, respectively. Smaller SW-sfc aerosol forcing values are found on 24 July

ACPD
9, 19387–19433, 2009

both over the Mediterranean Sea and the Italian peninsula. The daily SW-sfc aerosol forcing averaged over Europe and the Mediterranean Sea is −8 and −10 W/m^2 on 17 and 24 July, respectively (Table 1), while averaged over Sahara it is −33 and −35 W/m^2 on 17 and 24 July, respectively (Table 1).

The LW aerosol forcing is positive throughout the domain (Figs. 8 and 9) and over Africa daily values vary up to 110 and 50 W/m^2 at the surface and ToA, respectively. LW aerosol forcing values are significantly smaller over the Mediterranean where they vary within the 0–3 and 0–5 W/m^2 range at the ToA and surface, respectively. As a consequence, the LW aerosol forcing enhances the ToA radiative forcing over the dust sources and offsets the (negative) SW-ToA forcing away from them. The daily values of the LW aerosol forcing averaged both over the whole simulation domain and for the regions below and above 35° N are given in Table 1: on 17 July, the LW aerosol forcing offsets over Europe the (negative) ToA- and sfc-SW forcing by about 9%. Conversely, the LW aerosol forcing offsets the SW forcing averaged over Sahara by about 100% and 36% at the ToA and surface, respectively. On 24 July, the LW-ToA aerosol forcing averaged over the Sahara is 3.0 W/m^2, while the SW-ToA aerosol forcing is −2.6 W/m^2 (Table 1). Hence, model results indicate that the net-ToA aerosol radiative forcing is positive over Sahara when dust sources are activated and lead to AODs ≥0.8. Under these conditions, the net-ToA aerosol forcing thus enhances the ToA forcing due to greenhouse gases.

Ground based measurements of AOD and shortwave irradiance at the Mediterranean island of Lampedusa during 2003 and 2004 were recently used by di Sarra et al. (2008) to estimate daily average values of the SW-sfc aerosol radiative forcing. They found that at the equinox the average AOD at 496 nm was 0.35±0.1 and that the forcing was about of −24 W/m^2 for desert dust. Meloni et al. (2005) used an observation based radiative transfer model to calculate at Lampedusa daily average values of the SW aerosol forcing both at the ToA and surface during the Sahara dust outbreak on 18 May 1999. They found that the aerosol forcing was −27.6 and −3.6 W/m^2 at the surface and ToA, respectively. The measured AOD around 60° solar zenith angle was

ACPD
9, 19387–19433, 2009

0.49 at 550 nm. The above reported AODs and aerosol radiative forcing estimates are in satisfactory agreement with the RegCM3 estimates (Figs. 4a and 8–9) even if they refer to different dust outbreaks than the ones analyzed in this paper. Observation-based aerosol properties also were used by Tafuro et al. (2008) to initialize radiative transfer simulations. They found during the Sahara dust outbreak on 18 July 2005 that at Lecce instantaneous SW aerosol forcing at the ToA and surface of −21 and −38 W/m^2 at 16:49 UTC. The AOD at 550 nm was 0.32±0.01. These values are also consistent with the radiative forcing found in our work (see Figs. 8 and 9).

The instantaneous aerosol forcing is characterized by a larger variability range over the model domain. In particular, the instantaneous (12:00 UTC) SW aerosol forcing gets values up to 75 W/m^2 and −470 W/m^2, at the ToA and surface, respectively either on 17 and 24 July. Significantly larger instantaneous aerosol radiative forcing estimates have been reported by Perez et al. (2006) by analyzing a Saharan dust outbreak over the Mediterranean basin. They used a system based on the limited-area NCEP/Eta model as an atmospheric driver of the DREAM model for the simulation of a major dust outbreak that occurred in the Mediterranean region on 11–13 April 2002. According to Perez et al. (2006), instantaneous (12:00 UTC) AODs at 550 nm reach the value of 3.5 over the Algeria/Tunisia/Libya border on 12 April and vary within the 0.5–3 range over Italy. In addition they show that the instantaneous (12:00 UTC) SW-ToA forcing is positive both over Sahara and central Europe lands affected by dust intrusion, reaching values as high as 500 W/m^2. Conversely, the instantaneous (12:00 UTC) SW forcing at the surface is negative and reaches values smaller than −700 W/m^2 both over north-west Africa and Italy. LW aerosol forcing values by Perez et al. (2006) are also significantly larger than the one of this paper. The large modelled dust load is probably responsible for the high radiative effects by dust particle reported by Perez et al. (2006).

Table 1 provides main statistics of the daily-averaged SW aerosol forcing efficiency (FE) at the ToA and surface on 17 and 24 July, respectively. The aerosol FE is the radiative forcing produced by a unit of aerosol optical depth and is mainly dependent

ACPD
9, 19387–19433, 2009

on aerosol size and composition. The ToA-FE varies over Sahara from $-30\,W/m^2$ up to $50\,W/m^2$ both on 17 and 24 July. Conversely, the ToA-FE is always negative and varies within the $-(80-30)\,W/m^2$ range over the European areas affected by dust intrusion. The sfc-FEs varies within the $-(150-0)\,W/m^2$ range over the whole domain on 17 and 24 July, when the simulated AOD exceeds 0.1. Aerosol FE estimates are generally in line with previous reported values (e.g. Fouquart et al., 1987; Meloni et al., 2004; Helmert et al., 2007). Aerosol optical and microphysical properties are responsible for the different variability range of FEs over Sahara and Europe, as clearly revealed by Table 1, where mean FEs over Europe and Sahara are reported.

Daily-averaged SW atmospheric forcing (AF) values are plotted in Fig. 10a and c, for 17 and 24 July, respectively. The AF, defined as the difference between ToA and surface aerosol forcing at a solar wavelength, is an indicator of aerosol effects on the atmosphere energy budget. Figure 10 shows that the SW-AF values vary up to $250\,W/m^2$ over Africa's regions where AODs are highest (Fig. 2). Conversely, SW-AF values vary within the $3–30\,W/m^2$ range over the European regions affected by dust intrusion (Meloni et al., 2005).

5 Aerosol radiative feedbacks

A simulation (Exp1) including the aerosol model without accounting for its radiative feedback was performed in order to isolate the effects of the interactive aerosol online feedback. To this end, aerosol column burden, direct radiative forcing, and meteorological parameter values in the REF- and the Exp1-simulation were analyzed and compared. Daily-averaged aerosol column burden (CB) values (g/m^2) relating to the REF simulation are shown in Fig. 11a and b for 17 and 24 July, respectively. The differences between REF and Exp1 aerosol CB values are plotted in Fig. 11c and d for 17 and 24 July, respectively. The REF aerosol CB reaches values up to $18\,g/m^2$ over the main dust sources on 17 and 24 July and takes values below $1\,g/m^2$ over the Mediterranean Sea and Europe. This is in satisfactory agreement with the results by Helmert

ACPD
9, 19387–19433, 2009

et al. (2007), who used a model system consisting of the chemistry-transport model MUSCAT with a dust emission scheme to simulate the Saharan dust outbreak of 13 October 2001, which affected the central-west Mediterranean and central Europe.

Color-coded plots showing the daily-averaged differences between REF and Exp1 aerosol CB values (Fig. 11c and d) are very patchy: aerosol CB differences take positive and negative values that are comparable to the total aerosol CB values either over Sahara or Europe. In fact, aerosol CB differences vary over the Sahara dust sources (Fig. 1) from about $-16\,g/m^2$ up to $18\,g/m^2$. Conversely, CB differences vary over Europe from $-0.25\,g/m^2$ up to $0.25\,g/m^2$ and from $-0.50\,g/m^2$ up to $0.25\,g/m^2$ on 17 and 24 July, respectively. Aerosol effects on the atmospheric dynamics and hence on dust production and advection toward Europe are responsible for the marked dependence of aerosol CB values on simulation assumptions over the whole simulation domain. In addition, some differences between the aerosol CB in the two simulations are due to the internal model variability (Giorgi and Bi, 2000). Similar results have also been obtained by Heinold et al. (2007).

The domain-averaged aerosol CB difference is -0.1 and $-0.09\,g/m^2$ on 17 and 24 July, respectively, despite the large values of local CB differences (Tables 1–2). Hence, the interactive aerosol with the RegCM3 radiation scheme decreases the daily-averaged aerosol CB over the model domain by about 14% and 12% on 17 and 24 July, respectively. Since surface wind speeds did not change markedly between the interactive and non-interactive cases (not shown), the decreased CB is associated with less efficient dust production induced by increased stability due to dust-forced surface cooling (Zhang et al., 2009).

Daily-averaged 2 m-temperatures for the REF simulation are plotted in Fig. 12a and c for 17 and 24 July, respectively. The 2 m-temperature averaged over the whole simulation domain is 27.34 and 27.79°C on 17 and 24 July, respectively (Tables 1). Figure 12b and d show the 2 m-temperature differences (°C) between REF- and Exp1-simulation for 17 and 24 July, respectively. Temperature differences (ΔT) are quite dependent on location, generally following the CB differences. ΔT takes positive and negative values

ACPD
9, 19387–19433, 2009

and varies from about −8°C up to ∼3°C on 17 and 24 July, respectively. The 2 m-temperature differences averaged over the simulation domain are $\Delta T = -0.52$°C and $\Delta T = -0.39$°C on 17 and 24 July, respectively.

Daily-averaged vertical profiles of temperature (T), water vapor mixing ratio (MR), and wind speed (WS) at randomly selected sites are plotted in Figs. 13 and 14 to better highlight aerosol online feedback effects on atmospheric dynamics. Figure 13a–c shows T, MR, and WS vertical profiles of 17 July for the REF-case (black line) and the Exp1 simulation (grey line) at a selected north-west Sahara site: site 1 (36.10° N, 2.07° E, Fig. 10b). It is worth noting that T, MR, and WS vertical profiles are quite dependent on simulation assumptions. In particular, Fig. 13a shows that Exp1-temperatures (grey profile) are larger than REF-temperatures up to about 1.1 km then the differences between the two profiles reduce with altitude. This result shows that the aerosol online feedback increases the aerosol cooling effect in the lower troposphere, in accordance with Fig. 12b. REF-simulation MR values are slightly larger than corresponding Exp1-MRs up to about 3 km. Then, the differences between the two profiles reduce with altitude. WS vertical profiles are also quite dependent on simulation assumptions. Figure 13c shows that Exp1-WSs (grey profile) are significantly lower than corresponding REF-scenario-WSs at least up to about 7 km. Figure 13d–f shows the T, MR, and WS vertical profiles provided by the model on 17 July at a different north-west Sahara location: site 2 (27.76° N; 2.75° E, Fig. 10b). We observe that the interactive aerosol simulation (REF) produces in the lower troposphere lower temperatures and larger MR and WS values than the Exp1-simulation, in accordance with Fig. 13a–c.

Figure 14a–c and d–f show the T, MR, and WS vertical profiles provided by the REF-(black line) and Exp1-simulation (grey line) on 17 July at two randomly selected Italian sites located at 40.38° N–18.06° E (site 3) and at 42.40° N–12.43°E (site 4), respectively (Fig. 10b). The differences between REF and Exp1 profiles are on average smaller than the ones in Fig. 13. This is due to the fact that the radiative aerosol effects depend on the aerosol column burden, which over Italy is significantly smaller than that over the Sahara. In conclusion, Figs. 13 and 14 show that aerosol effects on atmospheric

ACPD
9, 19387–19433, 2009

dynamics may vary significantly within few tens of kilometers as a consequence of aerosol CB changes.

Figures 10b and d show the differences between daily-averaged SW-AF values by the REF- and the Exp1-simulation for 17 and 24 July, respectively. SW-AF differences significantly vary from site to site especially over the Sahara. As a consequence, aerosol effects on atmospheric dynamics may significantly change with location over the Sahara. Negative values of the SW-AF differences (Fig. 10b–d) indicate that the Exp1-simulation is responsible for an increase of the energy stored within the atmosphere and it is worth mentioning that larger atmospheric forcing values lead to a stabilizing effect of the atmospheric stratification. Daily-averaged SW-AF differences vary over Europe from −10 up to 10 W/m^2 and from −50 up to 10 W/m^2 on 17 and 24 July, respectively. Whereas, over the Sahara they vary from −180 up to 140 W/m^2 on 17 and 24 July, respectively. However, the SW-AF differences averaged over the Sahara lead to a mean difference of −4 W/m^2 on 17 and 24 July, respectively. Hence, the aerosol SW-AF mainly decreases over Africa if the aerosol online feedback on the radiation budget is accounted for. The comparison of Figs. 10b and 11c and of Figs. 10d and 11d clearly shows a strong relationship between SW-AF differences and aerosol CB differences.

The effects due to the aerosol direct radiative forcing can be inferred by comparing Fig. 8a and d and Fig. 15a and c. The last two figures show the 17 July daily-averaged SW radiative forcing at the ToA and surface, respectively for the Exp1-simulation. The differences between REF and Exp1 radiative forcing values are plotted in Fig. 15b and d for the ToA and surface, respectively. The comparison of Figs. 8d and 15c shows that on average the Exp1-simulation strengthens the aerosol radiative forcing at the surface. In fact, the REF and Exp1 SW radiative forcing, averaged over the whole simulation domain, is −24 and −25 W/m^2, respectively on 17 July at the surface. Conversely, the REF and Exp1 SW radiative forcing averaged over the whole domain is −3.4 and −3.2 W/m^2, respectively on 17 July at the ToA. However, the patchy pattern of Fig. 15b and d shows that the differences between REF and Exp1 values are locally significantly

ACPD
9, 19387–19433, 2009

larger both at the ToA and surface: atmospheric dynamics and hence dust production and advection processes are quite dependent on site and on simulation assumptions.

Figure 16a and c show the daily-averaged SW radiative forcing at the ToA and surface, respectively for 24 July and for the Exp1-simulation. The differences between REF and Exp1 values are plotted in Fig. 16b and d for the ToA and surface, respectively. The strengthening of the surface SW radiative forcing if the aerosol online feedback on the radiation budget is not accounted for is also revealed by Fig. 16d. The REF and Exp1 SW radiative forcing averaged over the whole domain is −24 and −25 W/m^2, respectively at the surface.

6 Interactive mineral dust radiative effects

A simulation without any desert aerosol affecting the radiation (Exp2) was performed to isolate the radiative forcing by mineral dust. Figures 17a and 17b show the Exp2-daily-averaged SW aerosol forcing at the ToA and surface, respectively for 17 July. The SW aerosol forcing by the SO_2/SO_4^{2-} system, hydrophobic and hydrophilic black carbon and organic carbon varies within the (−1.6–0.5) W/m^2 and −(4.5–0) W/m^2 at the ToA (Fig. 17a) and surface (Fig. 17b), respectively. The daily averaged LW aerosol forcing is close to negligible both at the ToA and surface. The comparison of Fig. 8a–b to Fig. 17a–b clearly shows the significant role of mineral dust on ToA and surface aerosol forcing. Exp2-SW aerosol forcing values averaged over the whole simulation domain and over the simulation domain above and below 35° N are given in Table 3, in addition to daily-averaged values of the AOD, aerosol CB, and 2 m-temperature. Table 3 shows that the aerosol forcing averaged over the whole simulation domain is −0.06 and −0.6 W/m^2 at the ToA and surface, respectively. Conversely, the REF-simulation SW aerosol forcing averaged over the whole domain is −3.4 and −24 W/m^2 at the ToA and surface, respectively. Figure 17c shows the 2 m-temperature differences between REF- and Exp2-simulation for 17 July. Temperature differences vary from −5°C to 3.5°C. However, the mean temperature difference over the whole simulation

ACPD
9, 19387–19433, 2009

above and below 35° N is −0.12, −0.02, and −0.16°C, respectively.

Interactive mineral aerosol effects on meteorological parameter vertical profiles can be inferred from Figs. 13 and 14 where *T*, MR, and WS vertical profiles for 17 July by the Exp2-simulation are plotted (dotted line). The *T*, MR, and WS vertical profiles in Exp2 are generally close to the corresponding ones in Exp1.

7 Summary and conclusion

The regional climate model RegCM3 coupled with a radiatively active aerosol model with online feedback on the radiation budget has been used to evaluate the aerosol radiative forcing of dust intrusion events over the Mediterranean basin. In particular, two major dust outbreaks with origin in north-west Sahara were analyzed, which occurred on 17 and 24 July 2003. Both dust outbreaks carried significant amounts of mineral dust over the central Mediterranean Sea and continental Europe. Even if several papers have been published on this subject, dust particles radiative effects are still not well parameterized in numerical models, as revealed by the differences between results from different models and between numerical and experimental data.

The RegCM3 simulation was first validated against a range of observations: AOD by satellite (MODIS) and AERONET sun/sky radiometer measurements, extinction coefficient vertical profiles by lidar measurements at selected Central Mediterranean sites. We find that RegCM3 is able to capture the dust outbreaks during July 2003, with a generally satisfactory agreement with observations. The main deficiency of the simulations is an underestimate of aerosol amounts at locations far from the dust source, particularly in the lower troposphere. This is an indication of weak long range transport, although a contribution to it is also given by an underestimate of background anthropogenic aerosols (probably related to the limited number of aerosol types in the model). Another factor affecting this result is likely the uncertainty in dust optical properties.

The simulation of SW and LW direct radiative forcing shows a prevalence of negative

ACPD
9, 19387–19433, 2009

values (cooling) at the surface both over the Sahara and Europe. Conversely, the daily net ToA forcing averaged over the Sahara is positive (0.4 W/m^2) or nearly close to zero for the two outbreaks of 24 and 17 July. This is a consequence of the offsetting effect of the LW-ToA direct aerosol forcing. We also found that the daily SW-ToA forcing is on average positive (up to 50 W/m^2) close to the source regions where the dust amounts are large. Over Europe, a negative net ToA-radiative effect is found.

The comparison of REF- and Exp1-simulation results illustrates the significant role of the aerosol online feedback on atmospheric dynamics and hence on dust production and advection toward Europe: local changes were significantly larger than domain-averaged changes. The daily-averaged aerosol CB decreases by 14 and 12% over the simulation domain on 17 and 24 July, if the aerosol online feedback on the radiation budget is accounted for, while, the daily-mean 2 m-temperature decreases by 0.52 and 0.39°C on 17 and 24 July, respectively. The analysis of daily-averaged vertical profiles of temperature, water vapor mixing ratio (MR), and wind speed (WS) at two randomly selected sites close to the dust sources shows that temperature decreases at least up to 1 km, while MR and WS increase at least up to 4 km if the aerosol online feedback is accounted for. In fact, the daily-averaged SW radiative forcing at the surface increases by about 7 and 2% over the whole simulation domain on 17 and 24 July, respectively, whereas the daily-averaged SW-AF decreases by 9 and 12% when including the aerosol online feedback. Finally, a sensitivity experiment without the inclusion of dust shows that Saharan dust is by far the greatest contributor to the total aerosol radiative forcing during dust outbreaks.

Our results show the importance of considering aerosol particles and corresponding radiative effects over the Mediterranean region. The aerosol effects on the atmosphere radiative budget may significantly change within few tens of kilometers following variations in the aerosol CB. Hence, the importance of using high resolution regional climate models to properly account for aerosol effects on climate is highlighted. Work is on progress to improve the aerosol parameterization in RegCM3 by also including sea-salt particles and a full treatment of organic aerosols.

ACPD
9, 19387–19433, 2009

Acknowledgement. M. Santese has carried out this work with the support of a post-doc fellowship by Centro euroMediterraneo per i Cambiamenti Climatici (CMCC). This work also has been supported by *Ministero dell' Istruzione dell'Università e della Ricerca* of Italy, (Programma di Ricerca di Interesse Nazionale 2006. Prot. 2006027825), by the European Project EARLINET-ASOS (2006 -2011, contract n. 025991), by Progetto FISR AEROCLOUDS. The authors kindly acknowledge Principal Investigators of the AERONET stations of Rome, Oristano, Etna, and Lampedusa. Dr. G. Gobbi is kindly acknowledged for providing lidar profiles at Etna's site.

References

Alfaro, S. C., and Gomes, L.: Modelling mineral aerosol production by wind erosion: Emission intensities and aerosol size distributions in source areas, J. Geophys. Res., 106, 18 075–18 084, 2001.

Andreae, T. W., Andreae, M. O., and Ichoku, C.: Light scattering by dust and anthropogenic aerosol at a remote site in the Negev desert, Israel, J. Geoph. Res., 107(D2), 4008, doi:10.1029/2001JD900252, 2002.

Balkanski, Y., Schulz, M., Claquin, T., and Guiber, S.: Reevaluation of Mineral aerosol radiative forcings suggests a better agreement with satellite and AERONET data, Atmos. Chem. Phys., 7, 81–95, 2007, http://www.atmos-chem-phys.net/7/81/2007/.

Bellantone, V., Carofalo, I., De Tomasi, F., Perrone, M. R., Santese, M., Tafuro, A. M., and Turnone, A.: In situ samplings and remote sensing measurements to characterize aerosol properties over South-East Italy, J. Atmos. Ocean. Technol., 25, 1341–1356, 2008.

Bergamo, A., Tafuro, A. M., Kinne, S., De Tomasi, F., and Perrone, M.: Monthly-averaged anthropogenic aerosol direct radiative forcing over the Mediterranean from AERONET derived aerosol properties, Atmos. Chem. Phys., 8, 6995–7014, 2008, http://www.atmos-chem-phys.net/8/6995/2008/.

Bergamo A., De Tomasi, F., and Perrone, M. R.: Direct radiative effects by anthropogenic particles at a polluted site: Rome (Italy), Nuovo Cimento, 31, 4, doi:10.1393/ncc/i2009-10320-1, 2009.

Chin, M., Kahn, R. A., and Swartz, S. E.: Atmospheric Aerosol Properties and Climate Im-

pacts, U.S. Climate Change Science Program (CCSP), Synthesis and Assessment Product 2.3, NASA Goddard Space Flight Center, 2009.
De Tomasi, F. and Perrone, M. R.: Lidar measurements of tropospheric water vapor and aerosol profiles over southeastern Italy, J. Geophys. Res. 108, 4286–4297, 2003.
De Tomasi, F., Tafuro, A. M., and Perrone, M. R.: Height and seasonal dependence of aerosol optical properties over south-east Italy, J. Geophys. Res., 111, D10203, doi:10.1029/2005JD006779, 2006.
Dickinson, R. E., Henderson-Sellers, A., and Kennedy P. J.: Biosphere-Atmosphere Transfer Scheme (BATS) version 1E as coupled to the NCAR Community Climate Model, NCAR Tech. rep. TN-387+STR, 72 pp., 1993.
Di Sarra, A., Pace, G., Meloni, D., De Silvestri, L., Piacentino, S., and Monteleone, F.: Surface shortwave radiative forcing of different aerosol types in the central Mediterranean, Geophys. Res. Lett., 35, L02714, doi:10.1029/2007GL032395, 2008.
Dubovik, O. and King, M. D.: A flexible inversion algorithm for retrieval of aerosol optical properties from Sun and sky radiance measurements, J. Geophys. Res., 105, 20 673–20 696, 2000.
Fouquart, Y., Bonnel, B., Broigniez, G., Buriez, J. C., Smith, L., Morerette, J. J., and Cerf, A. : Observations of Saharan aerosols: Results of ECLATS field experiment. Part II: broandband radiative characteristics of the aerosols and vertical radiative flux divergence, J. Clim. Appl. Meteorol., 26, 38–52, 1987.
Giorgi, F. and Bi, X. Q.: A study of internal variability of a regional climate model, J. Geophys. Res., 105(D24), 29 503–29 521, 2000.
Giorgi F.,: Climate change hot-spots, Geophys. Res. Lett., 33(8), L08707, doi:10.1029/2006GL025734, 2006.
Gobbi, G. P., Barnaba, F., Giorgi, R., and Santacasa, A.: Altitude-resolved properties of a Saharan-Dust event over the Mediterranean, Atmos. Environ., 34, 5119–5127, 2000.
Grell, G. A.: Prognostic evaluation of assumptions used by cumulus parameterizations, Mon. Weather Rev., 121, 2814–2832, 1993.
Grell, G. A., Dudhia, J., and Stauffer, D. R.: A description of the fifth-generation Penn State-NCAR Mesoscale Model (MM5). NCAR Tech. Note NCAR/TN-398+STR, National Center for Atmospheric Research, Boulder, Colorado, 122 pp., 1994.
Helmert, J., Heinold, B., Tegen, I., Hellmuth, O., and Wendisch, M.: On the direct and semidirect effects of Saharan dust over Europe: A modeling study, J. Geeophys. Res., 112, D13208,

doi:10.1029/2006JD007444, 2007.
Heinold, B., Helmert, J., Hellmuth, O., Wolke, R., Ansmann, A., Marticorena, B., Laurent, B., and Tegen, I. :Regional modeling of Saharan dust events using LM-MUSCAT: Model description and case studies, J. Geophys. Res., 112, D11204, doi:10.1029/2006JD007443, 2007.
Holtslag, A. A. M., de Bruijn, E. I. F., and Pan, H. L.: A high resolution air mass transformation model for short-range weather forecasting, Mon. Weather Rev., 118, 1561–1575, 1990.
Kalnay, E., et al.: The NCEP/NCAR 40-year reanalysis project, Bull. Am. Meteorol. Soc., 77, 437–471, doi:10.1175/1520-0477, 1996.
Kiehl, J. T., et al.: Description of the NCAR Community Climate Model (CCM3), NCAR Technical Notes, NCAR/TN-420+STR, 152 pp., 1996.
King, M. D.,. Kaufman, Y. J, Menzel, W. P., and Tanré, D.: Remote sensing of cloud, aerosol and water vapor properties from the moderate resolution imaging spectroradiometer (MODIS), IEEE Trans. Geosci. Remote Sens., 30, 1–27, 1992.
Konare, A., Zakey, A. S., Giorgi, F., Rauscher, S., Ibrah, S., and Bi, X.: A regional climate modeling study of the effect of desert dust on the West African monsoon, J. Geophys. Res., 113, D12206, doi:10.1029/2007JD009322, 2008.
Lelieveld, J., Berresheim, H., Borrmann, S., Crutzen, P. J., and Dentener, F. J. and co-authors: Global air pollution crossroads over the Mediterranean, Science, 298, 794–799, 2002.
Marticorena, B. and Bergametti, G.: Modeling the atmospheric dust cycle: 1. Design of a soil derived dust emission scheme, J. Geophys. Res., 100, 16 415–16 430, 1995.
Meloni, D., di Sarra, A., Di Iorio, T., and Fiocco, G.: Influence of the vertical profile of Sahara dust on the visible direct radiative forcing, J. Quant. Spectrosc. Ra., 93, 397–413, 2005.
Meloni, D., di Sarra, A., Di Iorio, T., and Fiocco, G.: Direct radiative forcing of Saharan dust in the Mediterranean from measurements at Lampedusa Island and MISR space-borne observations, J. Geophys. Res., 109, D08206, doi:10.1029/2003JD003960, 2004.
Pal, J. S., Small, E. E., and Elthair, E. A. B.: Simulation of regional-scale water and energy budgets: Representation of subgrid cloud and precipitation processes within RegCM, J. Geophys. Res., 105, 29 579–29 594, 2000.
Pal, J. S., Giorgi, F., Bi, X., Elguindi, N., Solmon, F., Gao, X., Rauscher, S. A., Francisco, R., Zakey, A., Winter, J., Ashfaq, M., Syed, F. S., Bell, J. L., Diffenbaugh, N. S., Karmacharya, J., Konare, A., Martinez, D., da Rocha, R. P., Sloan, L. C., and Steiner, A.: Regional climate modelling for the developing world: The ICPT RegCM3 and RegCNER, Bull. Atmos. Meteorol. Soc., 88(9), 1395–1409, 2007.

Perez, C., Nickovic, S., Pejanovic, G., Baldasano, J. M., and Ozsoy, E.: Interactive dust-radiation modeling: A step to improve weather forecasts, J. Geophys. Res., 111, D16206, doi:10.1029/2005JD006717, 2006.

Santese, M., De Tomasi, F., and Perrone, M. R.: Advection patterns and aerosol optical and microphysical properties by AERONET over south-east Italy in the central Mediterranean, Atmos. Chem. Phys., 8, 1881–1983, 2008, http://www.atmos-chem-phys.net/8/1881/2008/.

Sokolik, I. N., Winker, D. M., Bergametti, G., Gilette, D. A., Carmichael, G., Kaufman, Y., Gomes, L., Schuetz, L., and Penner, J. E.: Introduction to special section: Outstanding problems in quantifying the radiative impacts of mineral dust, J. Geophys. Res., 106, 18 015–18 028, 2001.

Solmon, F., Giorgi, F., and Liousse, C.: Aerosol modeling for regional climate studies: application to anthropogenic particles and evaluation over a European/African domain, Tellus, 58B, 51–72, 2006.

Tafuro, A. M., Banaba, F., De Tomasi, F., Perrone, M. R., and Gobbi, G. P.: Saharan dust particle properties over the central Mediterranean, Atmos. Res., 81, 67–93, 2006.

Tafuro, A. M., Kinne, S., De Tomasi, F., and Perrone, M.: Annual cycle of aerosol direct radiative effect over southeast Italy and sensitivity studies, J. Geophys. Res., 112, doi:10.1029/2006JD008265, 2007.

Tafuro, A., De Tomasi, F., and Perrone M. R.: Remote sensing of aerosols by sunphotometers and lidar tecniques. In: Kim, Y. J., Platt, U. (Eds.), Advanced Environmental Monitoring, Springer, ISBN:978-1-4020-63636-3, Chapt. 14, Vol. XXII, 422 pp., 2008.

Tegen, I.: Modeling the mineral dust aerosol cycle in the climate system, Quaternary Sci. Rev., 22(18–19), 1821–1834, doi:10.1016/S0277-3791(03)00163-X, 2003.

Todd, M. C., bou Karam, D., Cavazos, C., Bouet, C., Heinold, B., Baldasano, J. M., Cautenet, Koren, I., Perez., C., Solmon, F., Tegen, I., Tulet, P., Washington, R., and Zakey, A.: Quantifyng uncertainty in estimates of mineral dust flux: An intercoparison of model performance over the Bodele Depression, northern Chad, J. Geophys. Res., 113, D24107, doi:10.1029/2008JD010476, 2008.

Yu, H., Kaufaman, Y. J., Chin, M., Feingold, G., Remer, L. A., Anderson, T. L., Balkanski, Y., Bellouin, N., Boucher, O., Cristopher, S., De Cola, P., Kahn, R., Koch, D., Loeb, N., Reddy, M. S., Chulz, M., and Takemura, T., Zhou, M.: A review of measurement-based assessments of the aerosol direct radiative effect and forcing, Atmos. Chem. Phys., 6, 613–666, 2006,

http://www.atmos-chem-phys.net/6/613/2006/.
USDA: Soil taxonomy, a basic system of Soil Classification for making and interpreting Soil Surveys, US Government Printing Office, Washington, USA, 869 pp., 1999.
Zakey, A. S., Solmon, F., and Giorgi, F.: Implementation and testing of a desert dust module in a regional climate model, Atmos. Chem. Phys., 6, 4687–4704, 2006, http://www.atmos-chem-phys.net/6/4687/2006/.
Zhang, D. F., Zakey, A. S., Gao, X. J., Giorgi, F., and Solmon, F.: Simulation of dust aerosol and its regional feedbacks over East Asia using a regional climate model, Atmos. Chem. Phys., 9, 1095–1110, 2009, http://www.atmos-chem-phys.net/9/1095/2009/.

Table 1. REF-simulation: daily-mean values of the short-wave (SW) and long-wave (LW) aerosol forcing at the top of the atmosphere (ToA) and surface (sfc), the SW forcing efficiency (FE) at the ToA and surface, the SW atmospheric forcing (AF), the aerosol optical depth (AOD), the aerosol column burden (CB), and the 2-m temperature averaged over the whole simulation domain (Wh-domain) and over the simulation domain located above 35° N (a-35° N) and below 35° N (b-35° N) for 17 and 24 July 2003.

	17 July			24 July		
Parameters	Wh-domain	a-35° N	b-35° N	Wh-domain	a-35° N	b-35° N
SW-ToA (W/m^2)	−3.4	−3.9	−3.0	−3.5	−4.9	−2.6
SW-sfc (W/m^2)	−24	−8	−33	−25	−10	−35
LW-ToA (W/m^2)	1.9	0.3	3.0	1.9	0.4	3.0
LW-sfc (W/m^2)	7.6	0.8	12.2	8.4	0.9	13.6
FE-Toa (W/m^2)	−11	−19	−5	−11	−18	−6
FE-sfc (W/m^2)	−76	−108	−54	−80	−114	−57
AF (W/m^2)	20	4	30	21	5	32
AOD	0.52	0.14	0.78	0.54	0.17	0.79
CB (g/m^2)	0.63	0.09	0.99	0.63	0.09	1.0
T (°C)	27.34	20.46	32.00	27.79	20.87	32.48

ACPD
9, 19387–19433, 2009

Table 2. Exp1-simulation: daily-mean values of the short-wave (SW) and long-wave (LW) aerosol forcing at the top of the atmosphere (ToA) and surface (sfc), the SW forcing efficiency (FE) at the ToA and surface, of the SW atmospheric forcing (AF), the aerosol optical depth (AOD), the aerosol column burden (CB), and the 2-m temperature averaged over the whole simulation domain (Wh-domain) and over the simulation domain located above 35° N (a-35° N) and below 35° N (b-35° N) for 17 and 24 July 2003, respectively.

	17 July			24 July		
Parameters	Wh-domain	a-35° N	b-35° N	Wh-domain	a-35° N	b-35° N
SW-ToA (W/m^2)	−3.2	−3.8	−2.7	−3.5	−4.9	−2.6
SW-sfc (W/m^2)	−25	−8	−37	−25	−8	−37
LW-ToA (W/m^2)	2.5	0.3	4.0	2.6	0.5	3.9
LW-sfc (W/m^2)	9.1	0.8	14.7	8.6	1.2	13.6
AF (W/m^2)	22	4	34	24	7	36
AOD	0.57	0.14	0.85	0.65	0.23	0.94
CB (g/m^2)	0.73	0.09	1.17	0.72	0.13	1.1
T (°C)	27.86	20.49	32.8	28.18	20.96	33.07

ACPD
9, 19387–19433, 2009

Table 3. Exp2-simulation: 17 July-daily averaged values of the short-wave (SW) aerosol forcing at the top of the atmosphere (ToA) and surface (sfc), the SW atmospheric forcing (AF), the aerosol optical depth (AOD), the aerosol column burden (CB), and of the temperature (T) averaged over the whole simulation domain (Wh-domain) and over the simulation domain located above 35° N (a-35° N) and below 35° N (b-35° N).

Parameters	Wh-domain	a-35° N	b-35° N
SW-ToA (W/m^2)	−0.06	−0.17	0.02
SW-sfc (W/m^2)	−0.6	−0.8	−0.4
AF (W/m^2)	0.5	0.6	0.4
AOD	0.006	0.007	0.006
CB (g/m^2)	0.0012	0.0010	0.0014
T (°C)	27.46	20.48	32.16

ACPD
9, 19387–19433, 2009

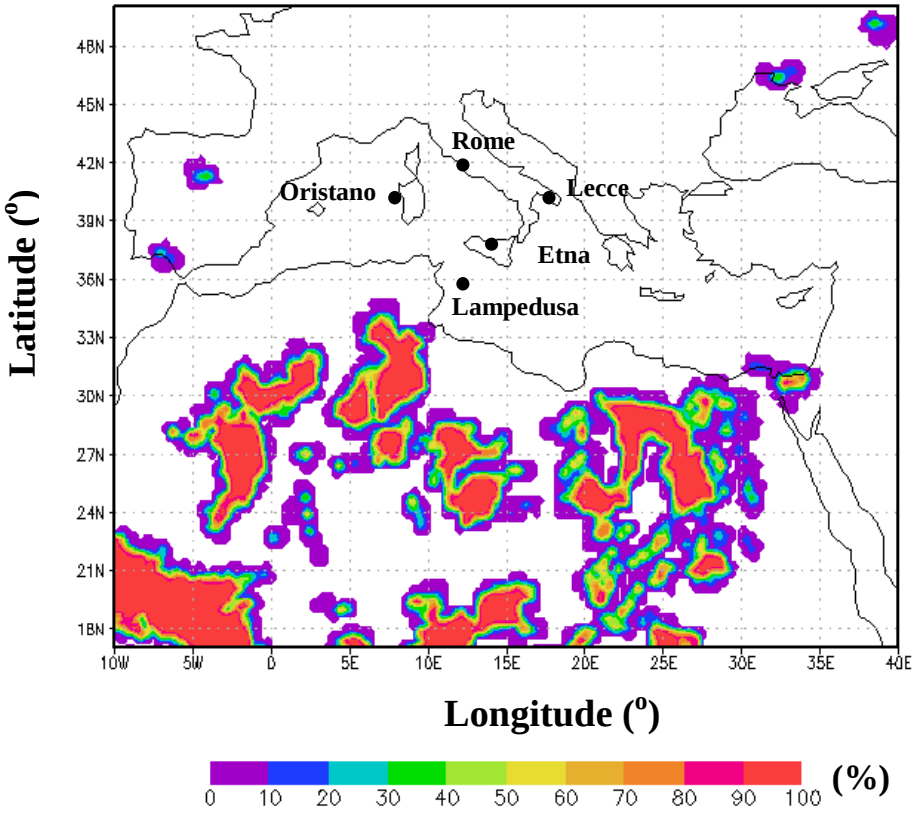

Fig. 1. Sand source percentages inside the model domain. Full dots indicate the location of some Italian AERONET sites.

ACPD

9, 19387–19433, 2009

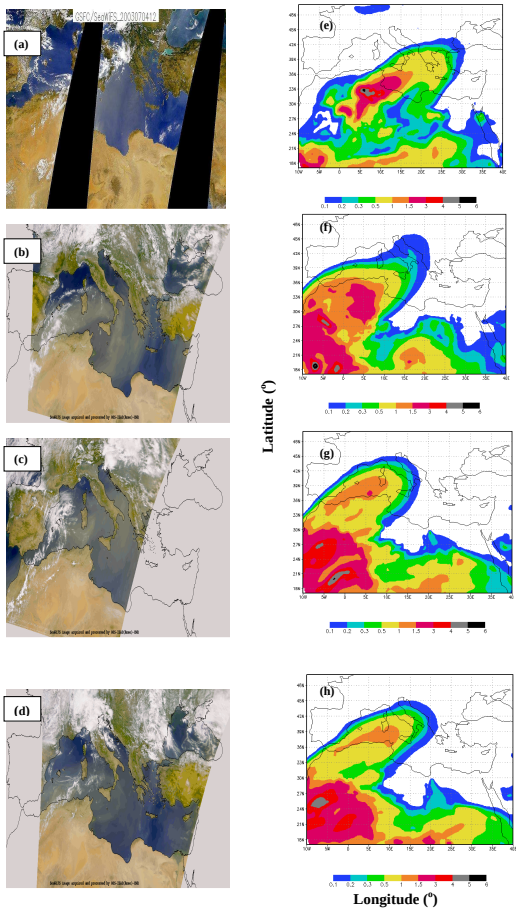

Fig. 2. (a–d) SeaWiFS true color images and **(e–h)** color-coded plots of simulated AODs (daily average) at the 350–640 nm model band for 4, 17, 23, and 24 July 2003, respectively.

ACPD
9, 19387–19433, 2009

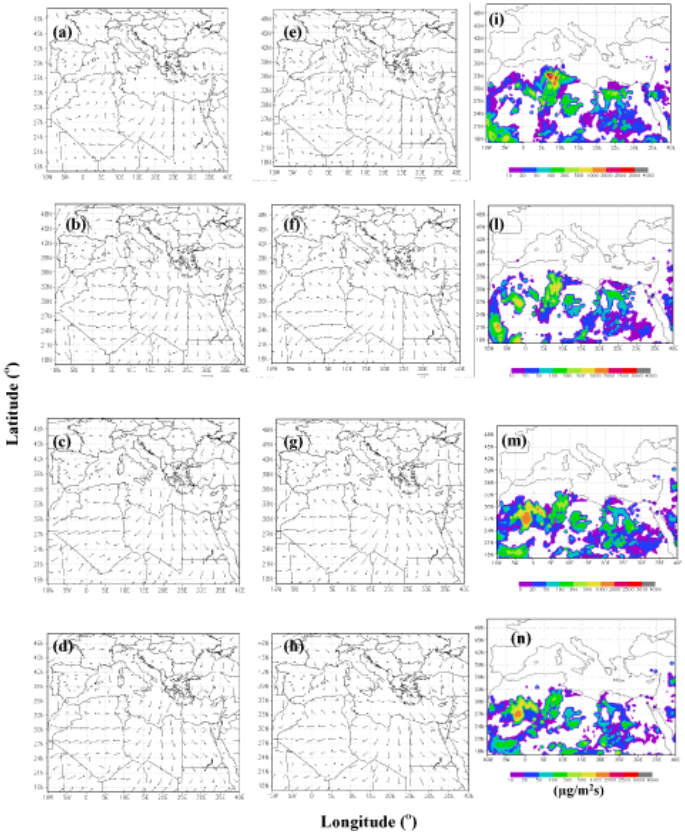

Fig. 3. Comparison between **(a–d)** RegCM3 simulated 10-m winds and **(e–h)** NCEP-NNRP2 reanalysis for 4, 17, 23 and 24 July 2003, respectively. Daily mean values of dust emission fluxes (μg/m^2 s) are shown in **(i–n)** by color coded plots for 4, 17, 23 and 24 July 2003, respectively.

ACPD
9, 19387–19433, 2009

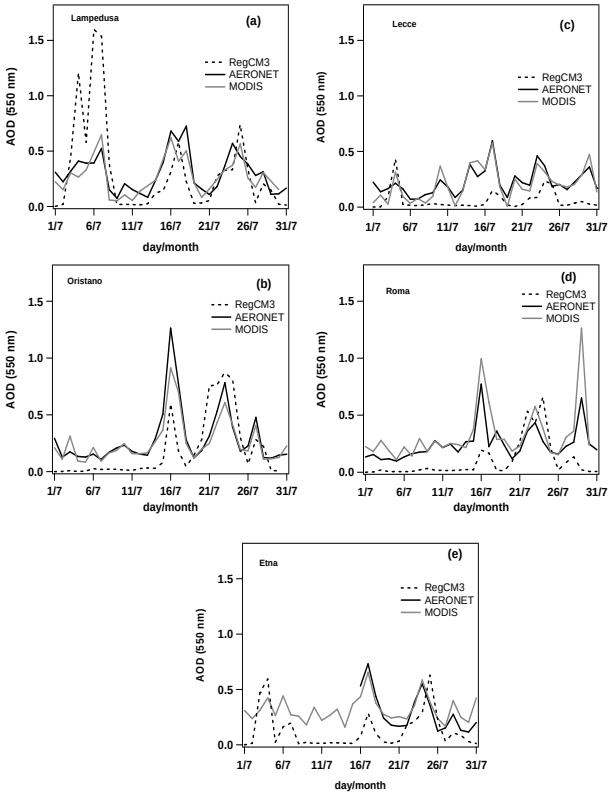

Fig. 4. AOD daily-mean-values for July 2003 from the model (dotted line), AERONET sun/sky radiometer measurements (black solid line), and MODIS satellite measurements (grey solid line) at **(a)** Lampedusa, **(b)** Oristano, **(c)** Lecce, **(d)** Rome, and **(e)** Etna.

ACPD
9, 19387–19433, 2009

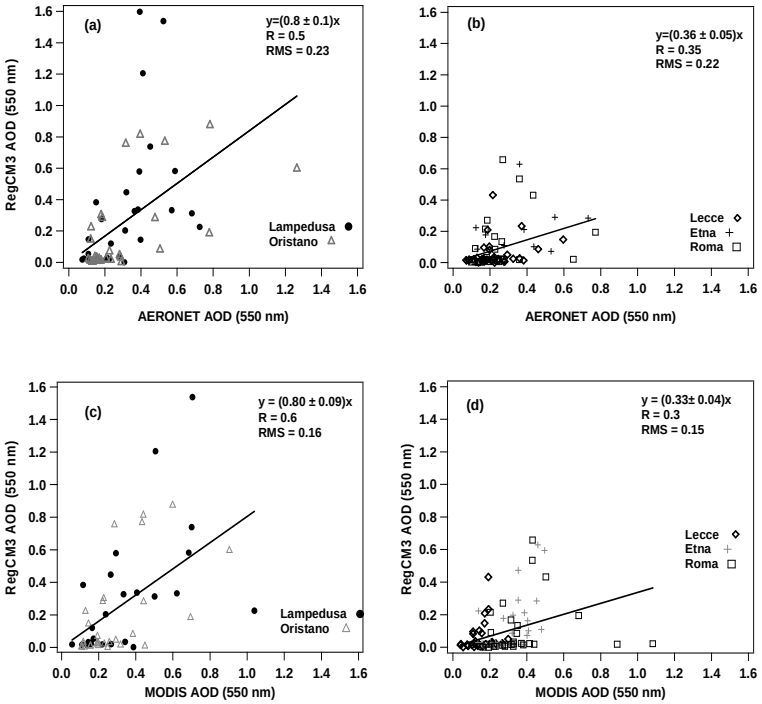

Fig. 5. Scatterplot of RegCM3-AODs versus AERONET-AODs retrieved **(a)** at Lampedusa (full dots) and Oristano (open triangles) and **(b)** at Lecce (rombs), Etna (crosses), and Rome (boxes). Scatterplot of RegCM3-AODs versus MODIS-AODs retrieved **(c)** at Lampedusa (full dots) and Oristano (open triangles) and **(d)** at Etna (crosses), Lecce (rombs), and Rome (boxes). The solid black line represents in each plot the linear regression line fitting the data points. Regression line slope and linear correlation coefficient (R) are also given in each plot in addition to the root mean square (RMS) difference.

ACPD
9, 19387–19433, 2009

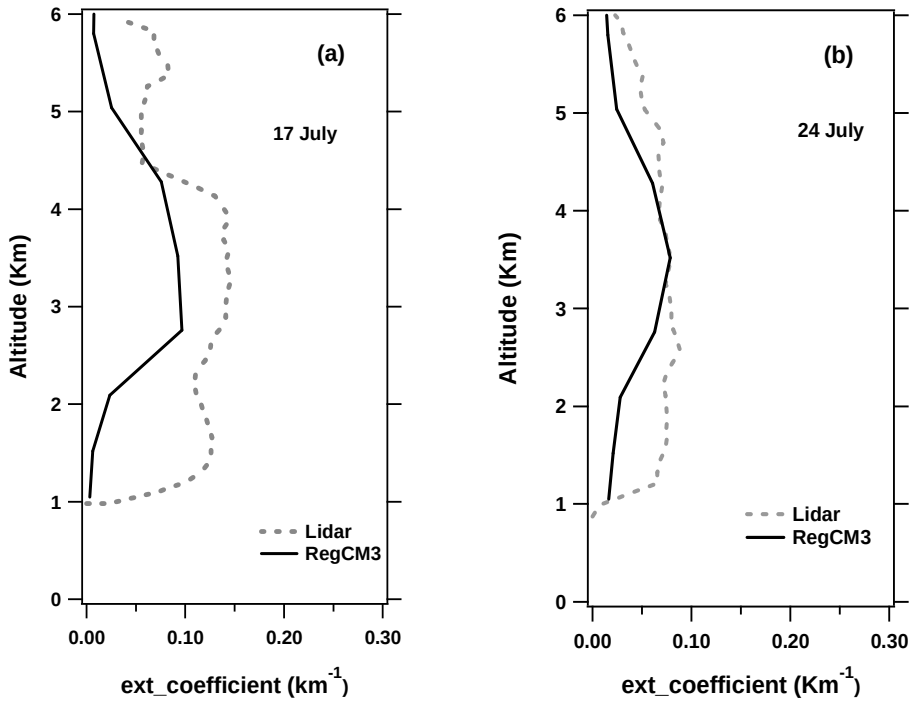

Fig. 6. Extinction coefficient profiles by RegCM3 (black line) and lidar measurements (grey dotted lines) at Etna on **(a)** 17 and **(b)** 24 July. In particular, the extinction coefficient profile retrieved by lidar measurements performed on 17 July from 14:05 to 14:15 UTC is compared in **(a)** to the RegCM3 extinction coefficient profile at 12:00 UTC. The 24 July extinction coefficient profile retrieved by lidar measurements from 19:30 to 19:40 UTC is compared in **(b)** with the one by RegCM3 at 18:00 UTC.

ACPD
9, 19387–19433, 2009

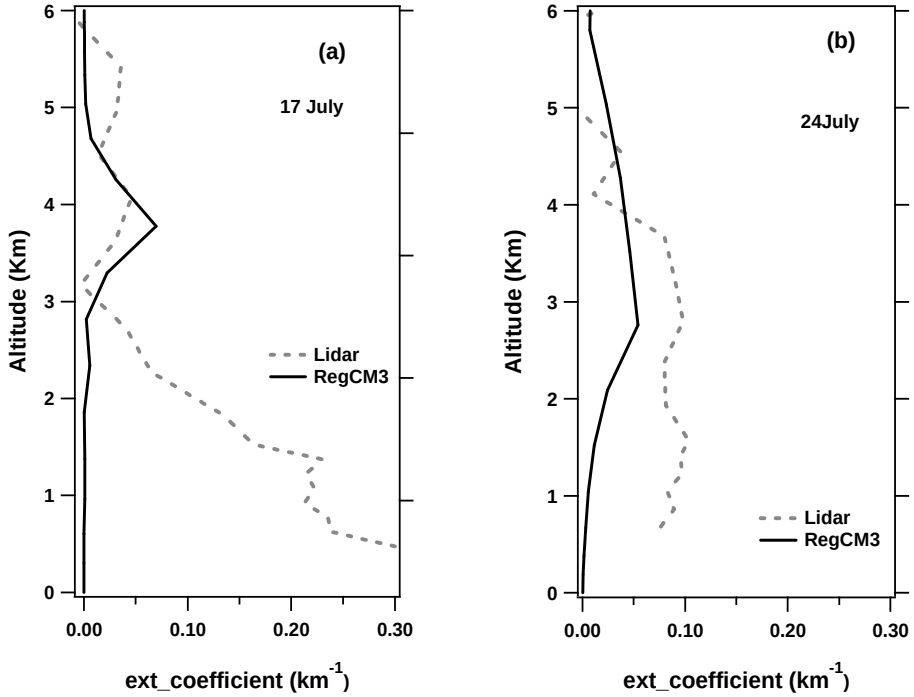

Fig. 7. Extinction coefficient profiles retrieved at Lecce on **(a)** 17 and **(b)** 24 July by lidar measurements (grey dotted lines) from 13:00 to 14:00 UTC and from 20:00 to 21:00 UTC, respectively. Black lines show the extinction coefficient profiles by RegCM3 at **(a)** 12:00 and **(b)** 18:00 UTC, respectively.

ACPD
9, 19387–19433, 2009

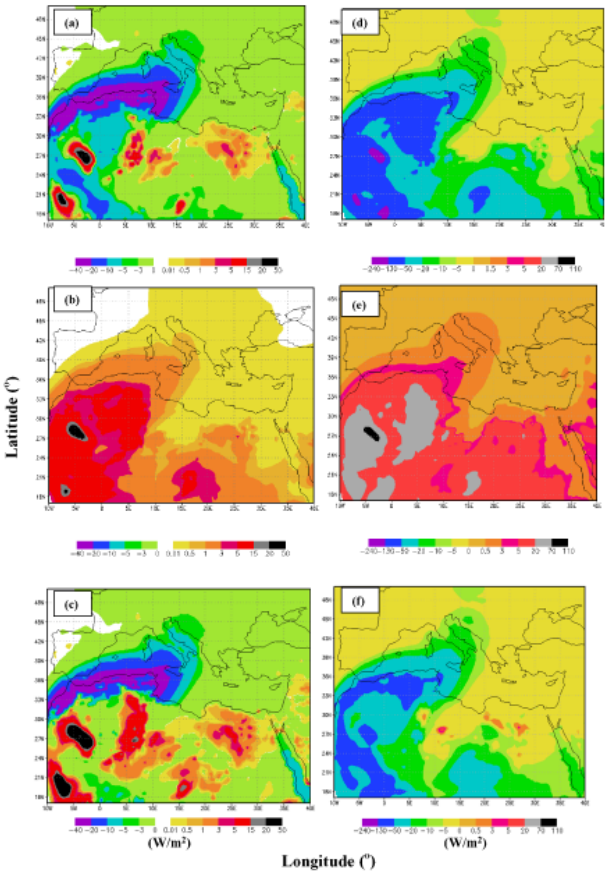

Fig. 8. 17 July 2003 daily mean values of the SW direct aerosol forcing (W/m^2) at the **(a)** ToA and **(d)** surface, of the LW direct aerosol forcing (W/m^2) at the **(b)** ToA and **(e)** surface, and of the net direct aerosol forcing (W/m^2) at the **(c)** ToA and **(f)** surface for the REF-experiment.

ACPD
9, 19387–19433, 2009

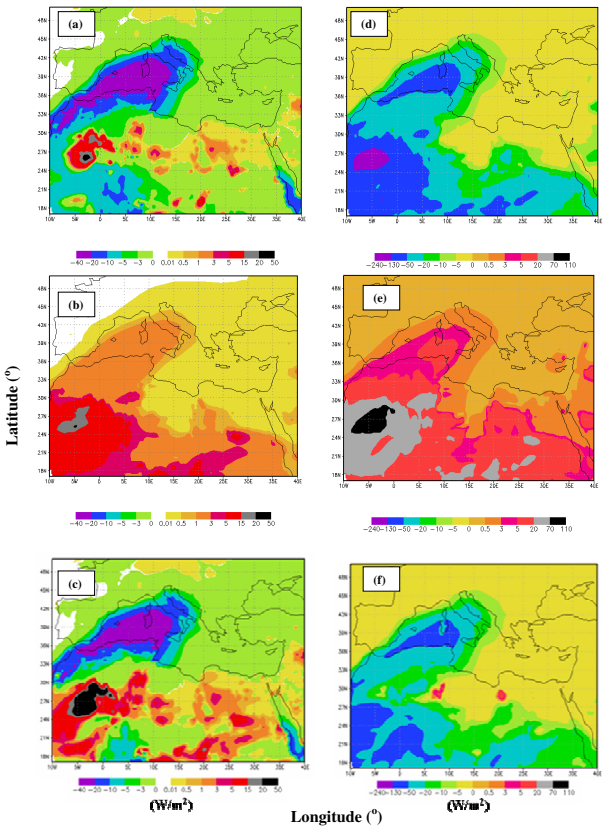

Fig. 9. 24 July 2003 daily mean values of the SW direct aerosol forcing (W/m^2) at the **(a)** ToA and **(d)** surface, of the LW direct aerosol forcing (W/m^2) at the **(b)** ToA and **(e)** surface, and of the net direct aerosol forcing (W/m^2) at the **(c)** ToA and **(f)** surface for the REF-experiment.

ACPD
9, 19387–19433, 2009

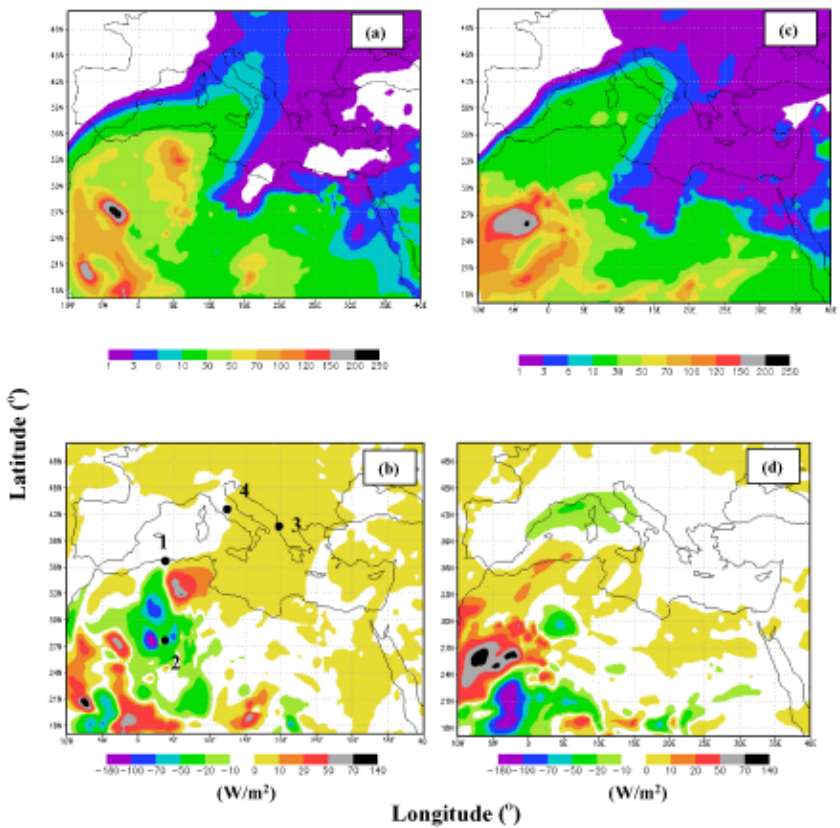

Fig. 10. REF-experiment: daily-averaged-values of the SW-atmospheric forcing (AF, W/m^2) for **(a)** 17 and **(c)** 24 July 2003; differences between REF and Exp1 SW-AF values (W/m^2) for **(b)** 17 and **(d)** 24 July. Full dots and corresponding numbers in Fig. 10b indicate the 4 sites where the simulated vertical profiles of T, MR and WS shown in Figs. 13 and 14 are provided.

ACPD
9, 19387–19433, 2009

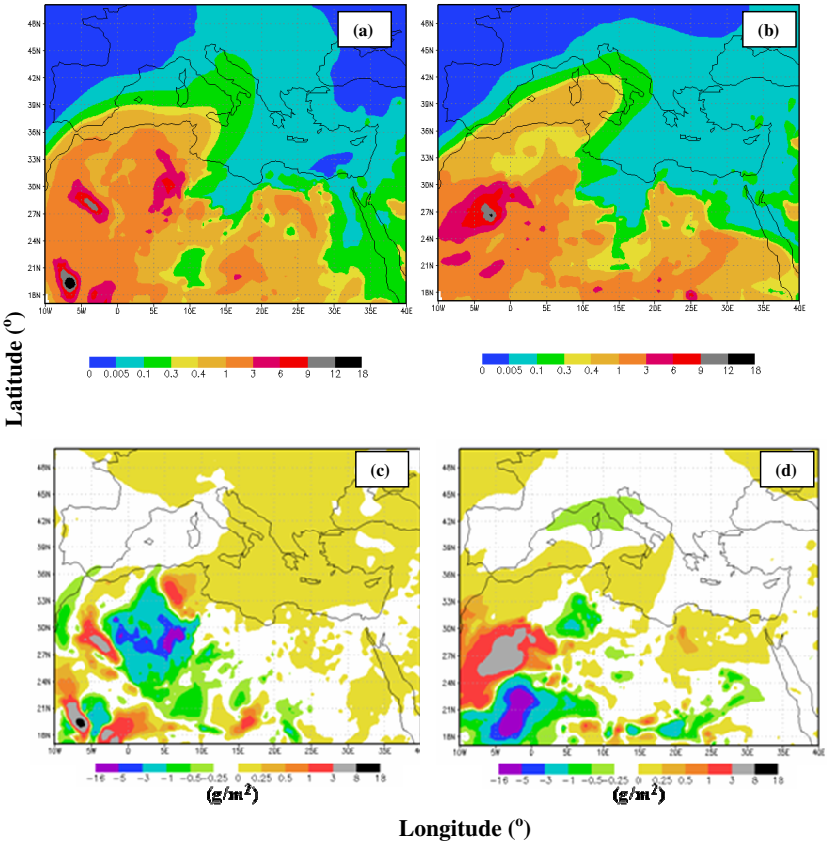

Fig. 11. REF-experiment: daily-averaged-values of the aerosol column burden (CB, g/m^2) for **(a)** 17 and **(b)** 24 July 2003. Differences between REF and Exp1 CB values for **(c)** 17 and **(d)** 24 July.

ACPD
9, 19387–19433, 2009

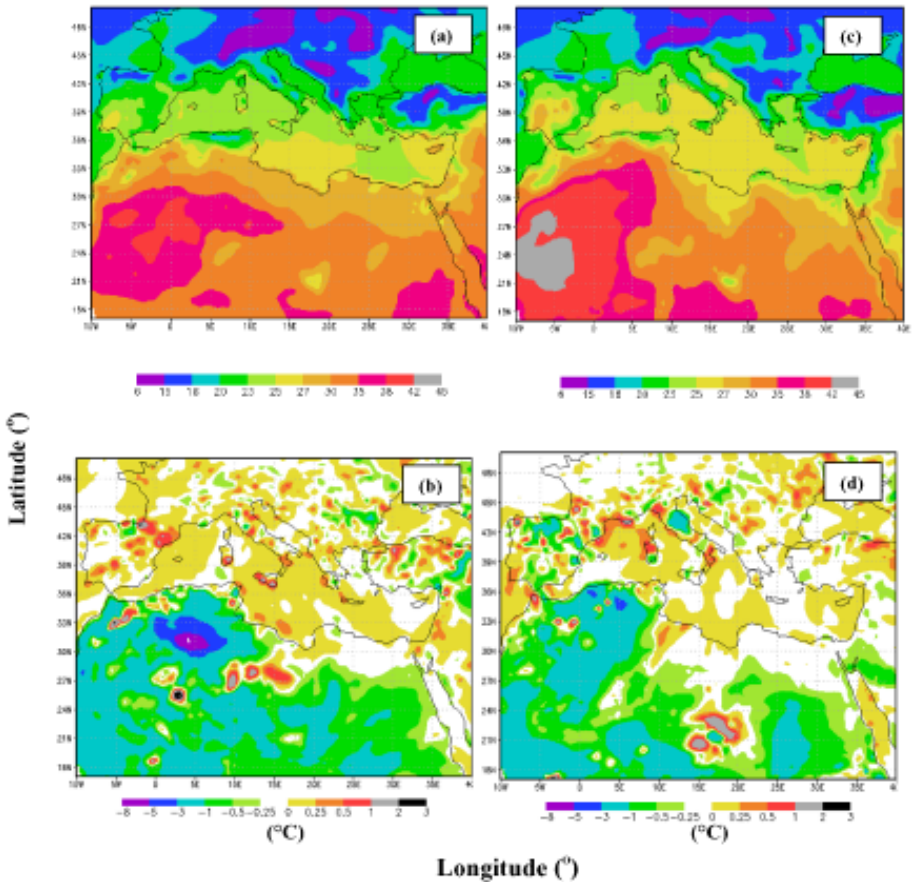

Fig. 12. REF-experiment: daily-averaged-values of the 2 m-temperature (°C) for **(a)** 17 and **(c)** 24 July 2003. Differences between REF and Exp1 2 m-temperature values for **(b)** 17 and **(d)** 24 July.

ACPD
9, 19387–19433, 2009

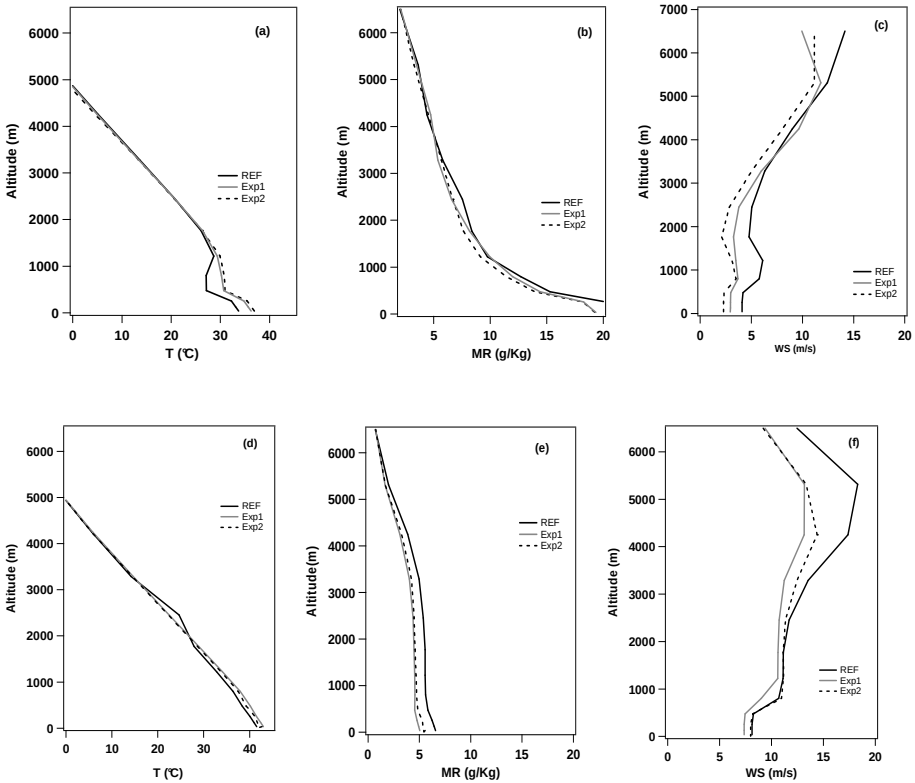

Fig. 13. Daily-averaged vertical profiles of temperature (T), water vapor mixing ratio (MR), and wind speed (WS) for 17 July 2003 at two selected north-west Africa sites: **(a–c)** site 1 (36.10° N, 2.07° E) and **(d–f)** site 2 (27.76° N, 2.75° E). Black-solid-line, grey-solid-line, and dotted-line relate to REF-, Exp1-, and Exp2-simulation, respectively.

ACPD
9, 19387–19433, 2009

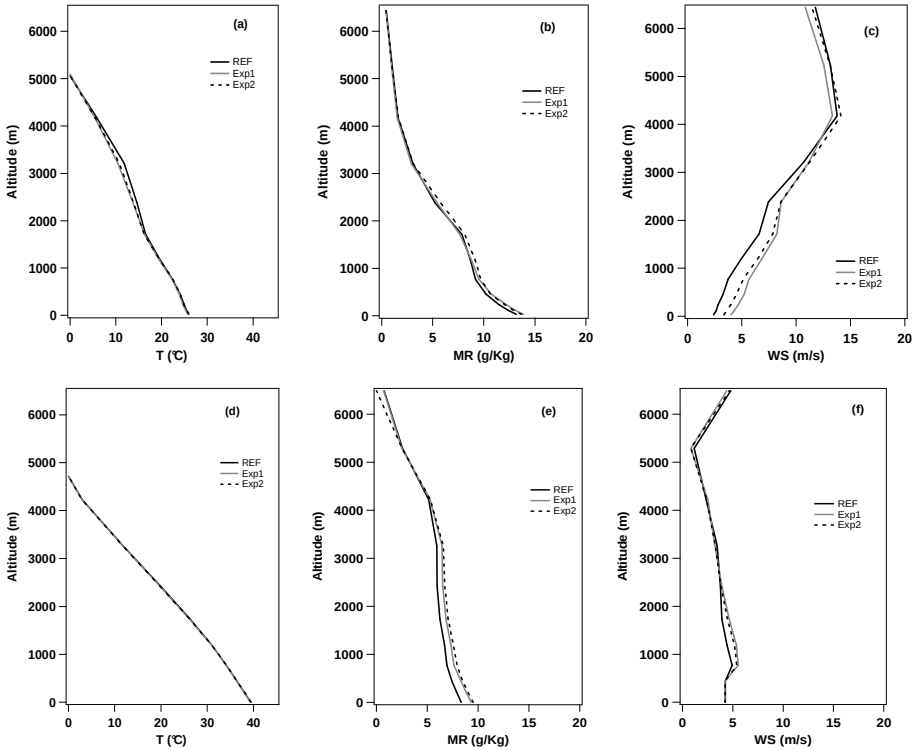

Fig. 14. Daily-averaged vertical profiles of temperature (T), water vapor mixing ratio (MR), and wind speed (WS) for 17 July 2003, at two selected Italian sites: **(a–c)** site 3 (40.38° N, 18.06° E) and **(d–f)** site 4 (42.40° N, 12.43° E). Black-solid-line, dotted-line, grey-solid-line, and dotted-line relate to REF-, Exp1-, and Exp2-simulation, respectively.

ACPD
9, 19387–19433, 2009

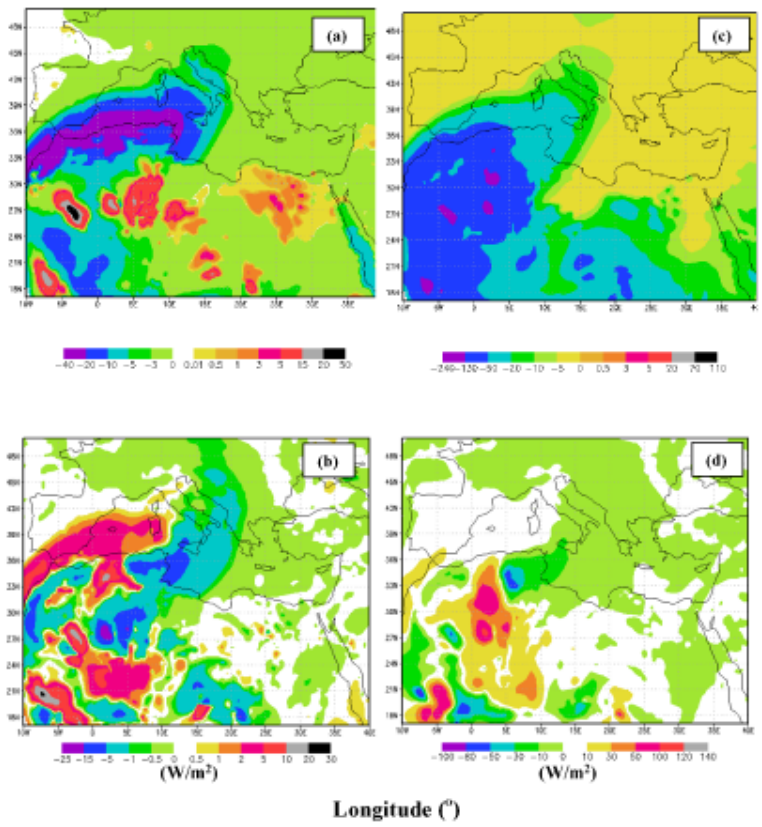

Fig. 15. Exp1-simulation: daily averaged values of the SW aerosol forcing (W/m^2) at the **(a)** ToA and **(c)** surface for 17 July 2003. Differences between REF and Exp1 SW aerosol forcing values at the **(b)** ToA and **(d)** surface.

ACPD

9, 19387–19433, 2009

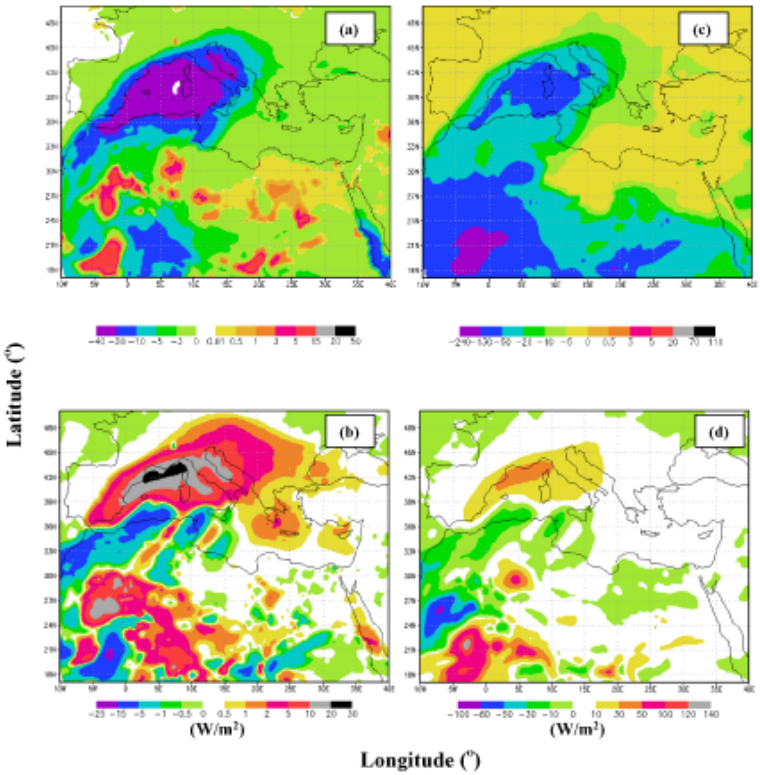

Fig. 16. Exp1-simulation: daily averaged values of the SW aerosol forcing (W/m^2) at the **(a)** ToA and **(c)** surface for 24 July 2003. Differences between REF and Exp1 SW aerosol forcing values at the **(b)** ToA and **(d)** surface.

ACPD

9, 19387–19433, 2009

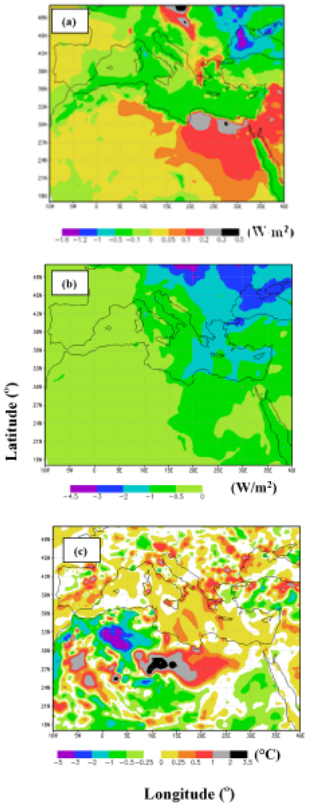

Fig. 17. Exp2-simulation: daily averaged values of the SW-forcing (W/m^2) at the **(a)** ToA and **(b)** surface on 17 July 2003. **(c)** Differences between REF and Exp2 2 m-temperature values (°C).

ACPD
9, 19387–19433, 2009